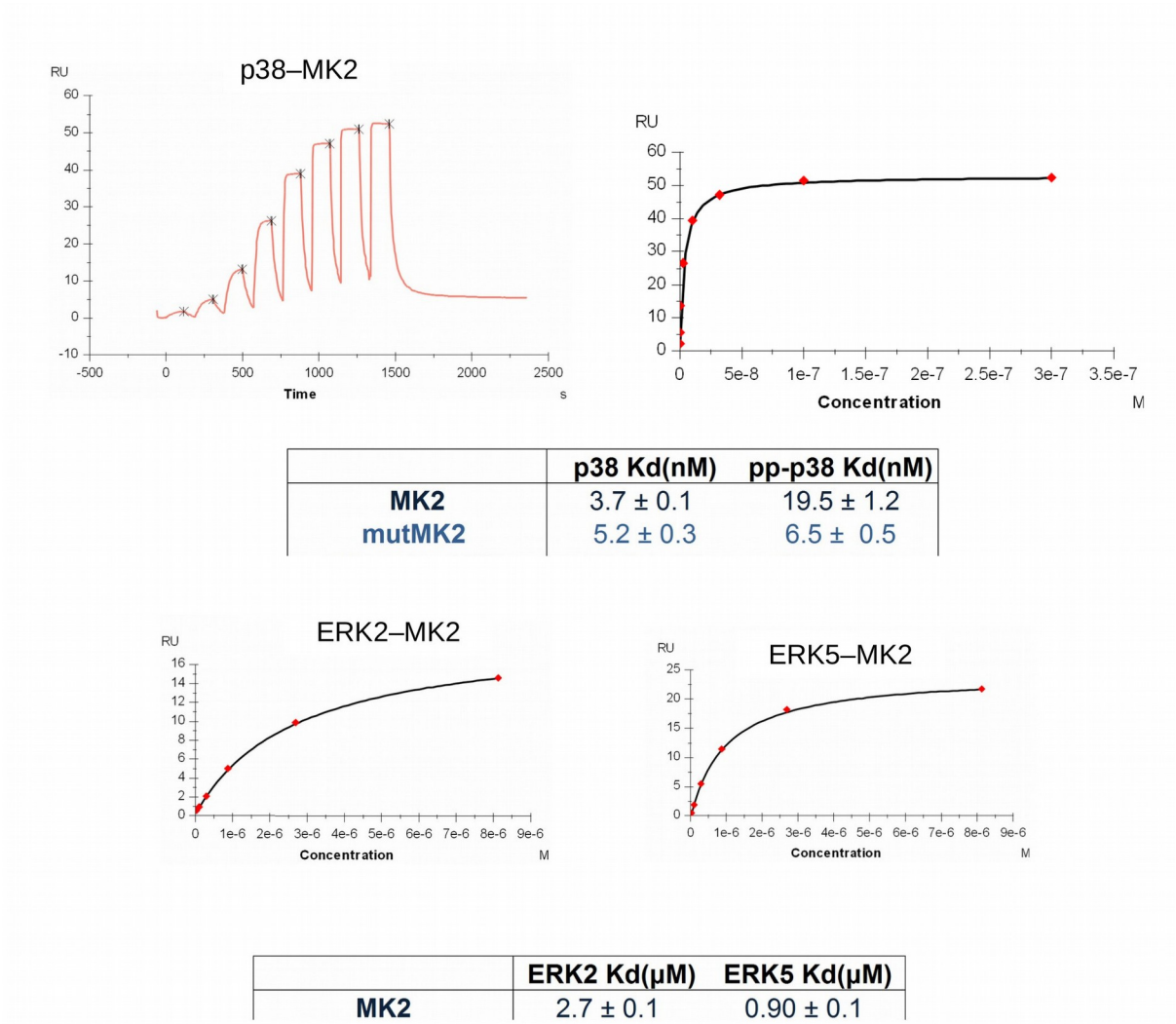

	p38 Kd(nM)	pp-p38 Kd(nM)
MK2	3.7 ± 0.1	19.5 ± 1.2
mutMK2	5.2 ± 0.3	6.5 ± 0.5

	ERK2 Kd(μM)	ERK5 Kd(μM)
MK2	2.7 ± 0.1	0.90 ± 0.1

Figure S1. Related to Figure 2. Results of surface plasmon resonance (SPR) measurements for MK2 containing complexes.

Upper panel on the left shows the results of a single-cycle titration experiment (after double referencing) in which increasing amounts of the analyte (MK2) was injected over the MAPK surface. The equilibrium RU binding curve is shown on the right. MAPKs (p38, pp-p38, ERK2 or ERK5) were produced biotinylated and captured on a Biacore CAP chip. The table contains the Kd values calculated from the binding curves for different p38-MK2 complexes. Note that p38-MK2 binding affinity is similar to that of the p38-mutMK2 complex (~5 nM). Binding plots below are shown for ERK2-MK2 and ERK5-MK2 similarly measured as described above. The table below shows the Kd values for these two complexes. Error bars indicate the standard error from two replicate measurements.

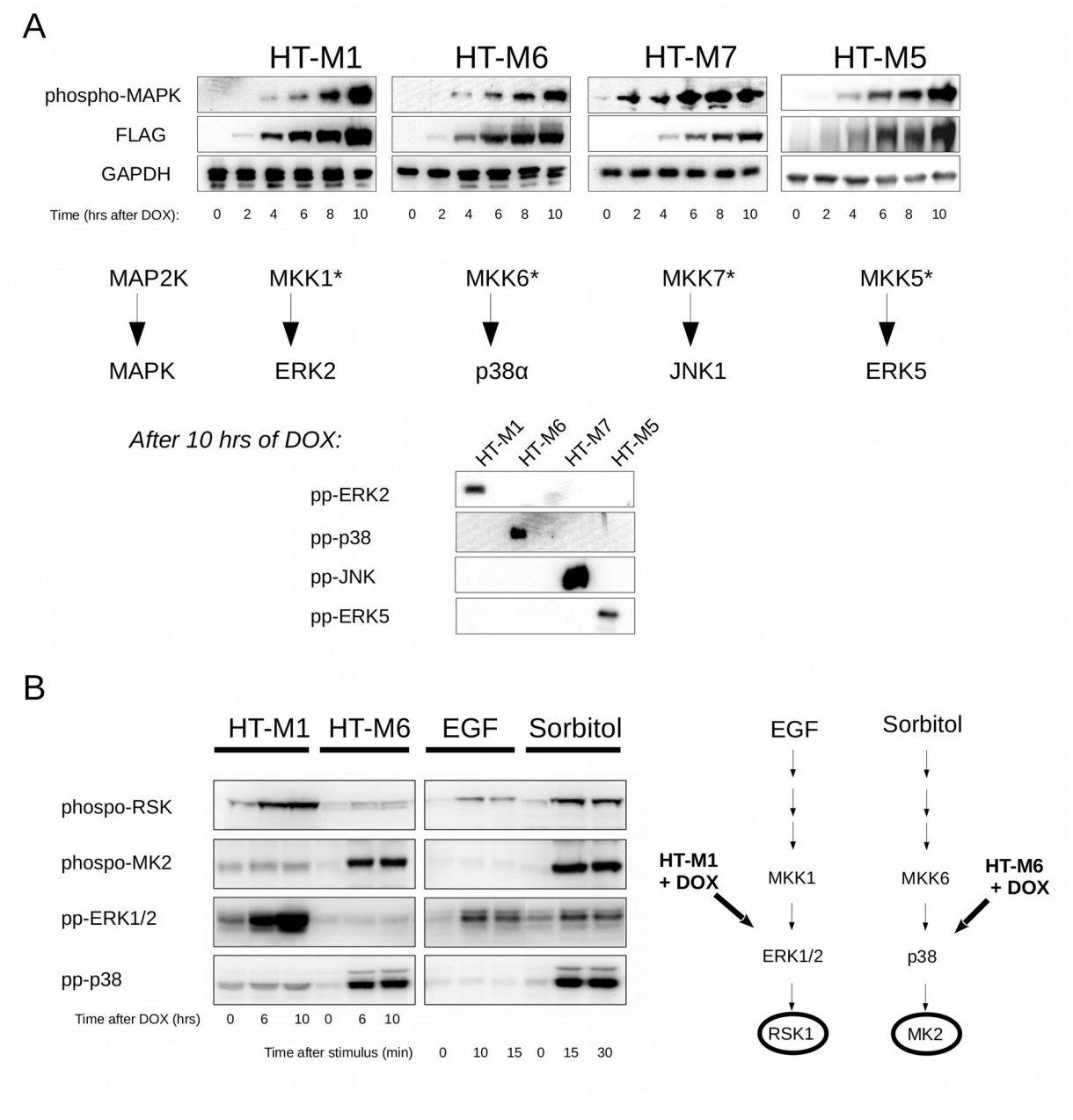

Figure S2. Related to Figure 2. HEK293T based "designer cells" for specific MAPK activation

(**A**) HT-M cells allow specific MAPK activation only one at a time and they contain high levels of ERK1/2 and p38. Activation of these endogenous MAPKs was monitored by using phospho-specific antibodies from cell lysates. Endogenous JNK and ERK5 levels in 293T cells are low, therefore HT-M7 and HT-M5 cells were transfected with JNK1 and ERK5 expressing constructs, respectively. (HT-M7 cells were not used in this study as JNK cannot activate MAPKAPKs directly due to its narrowed MAPK docking groove that cannot accept MAPKAPK linear motifs (Garai et al, 2012). Note that the lower phospho-MAPK Western-blot panels demonstrate specific MAPK activation in HT-M cells after DOX treatment. The system exploits the uniquely high degree of specificity between MAP2Ks and their cognate MAPK substrates.

(**B**) Phosphorylation of RSK1 and MK2 in HT-M1 and HT-M6 cells. Activation of endogenous RSK1 or MK2 was monitored by phospho-MAPKAPK Western-blots after addition of doxycycline (left panels). DOX induced RSK1 and MK2 phosphorylation was compared to when cells were stimulated by EGF (50 ng/mL) or sorbitol (0.5M), respectively. Notice that EGF elicits ERK-RSK specific activation, while sorbitol treatment turns on both p38 and ERK1/2 pathways. In contrast, the use of HT-M cells allows specific MAPK and thus specific downstream kinase activation, devoid of any lateral signal spread observed after sorbitol treatment for example.

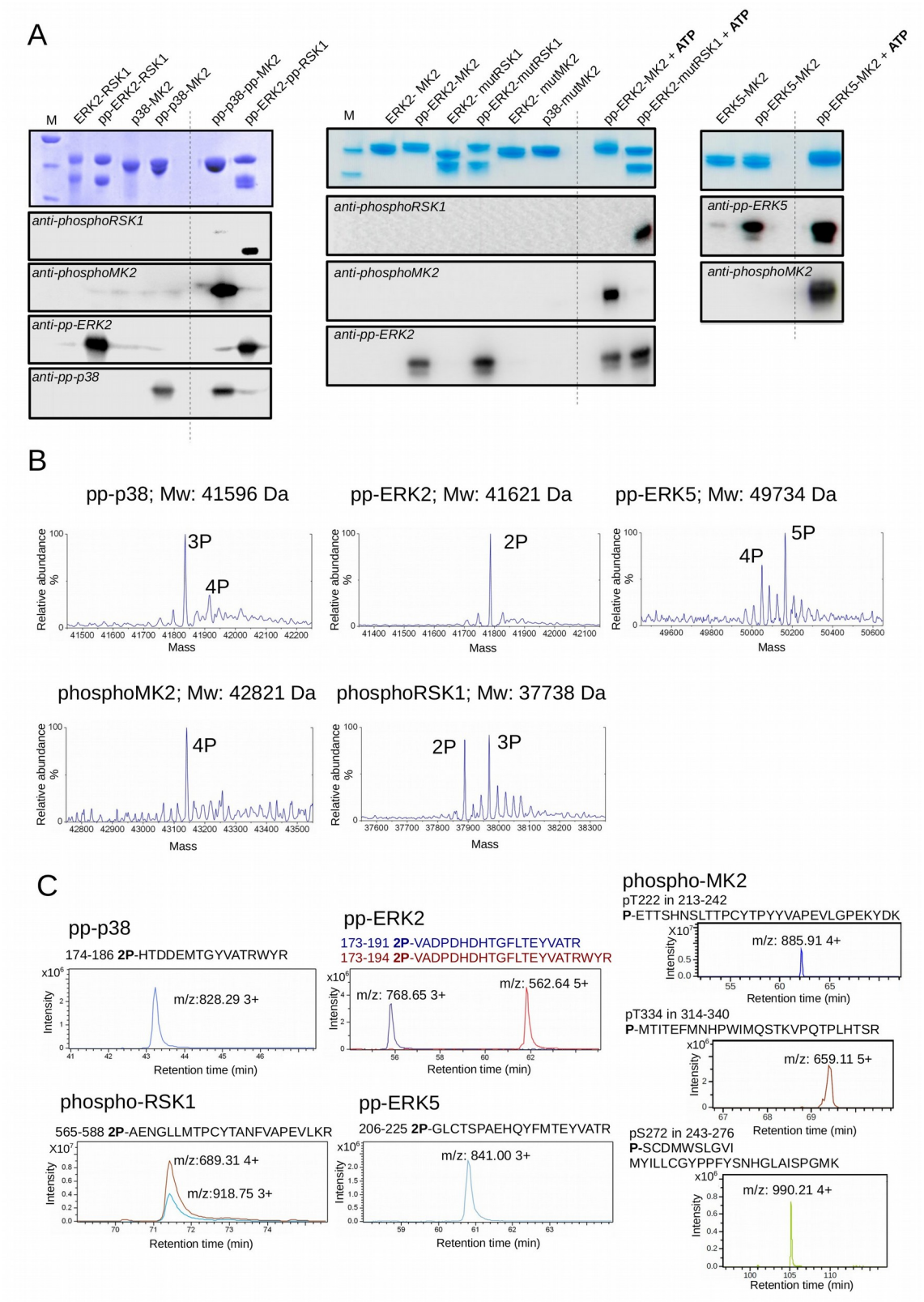

Figure S3. Related to Figure 2. Characterization of protein samples by Western-blots and mass spectrometry

(**A**) Coomassie stained SDS-PAGE of gel filtrated MAPK-MAPKAPK heterodimers (upper panels). (Unfortunately, MK2 runs close to all MAPKs, and the two protein bands from MAPK-MK2 complexes are barely discernible.) After gel filtration, samples were concentrated to ~8 mg/ml and 1 µL was loaded on the gel. The phosphorylation state of the prepared samples was confirmed by Western-blots using activation loop phosphorylation specific antibodies (phosphoRSK1, phosphoMK2, pp-ERK2 or pp-p38). ATP was added to active heterodimers and incubated at room temperature for 1 hour in kinase buffer to demonstrate the intact function of assembled heterodimers. In addition, these phosphorylated samples – where MAPK and MAPKAPK were both phosphorylated – were also analyzed by SAXS.
(**B**) Mass analysis of intact proteins: the molecular weight of phosphorylated proteins was determined using HPLC-MS. The deconvoluted mass spectra show that all protein samples were at least double-phosphorylated. Mw – expected molecular weight of nonphosphorylated proteins.
(**C**) Ion-chromatograms of functionally relevant peptides corresponding to protein regions (e.g. kinase activation loop) regulated by phosphorylation. Phosphorylated protein samples were trypsin digested. The phosphorylation is confirmed by the ion chromatogram of phosphorylated peptides.

Note that activated MK2 is known to be phosphorylated on residues outside of its activation loop (on Ser^{272} and Thr^{334}, in addition to Thr^{222}). These sites were also found to be phosphorylated.

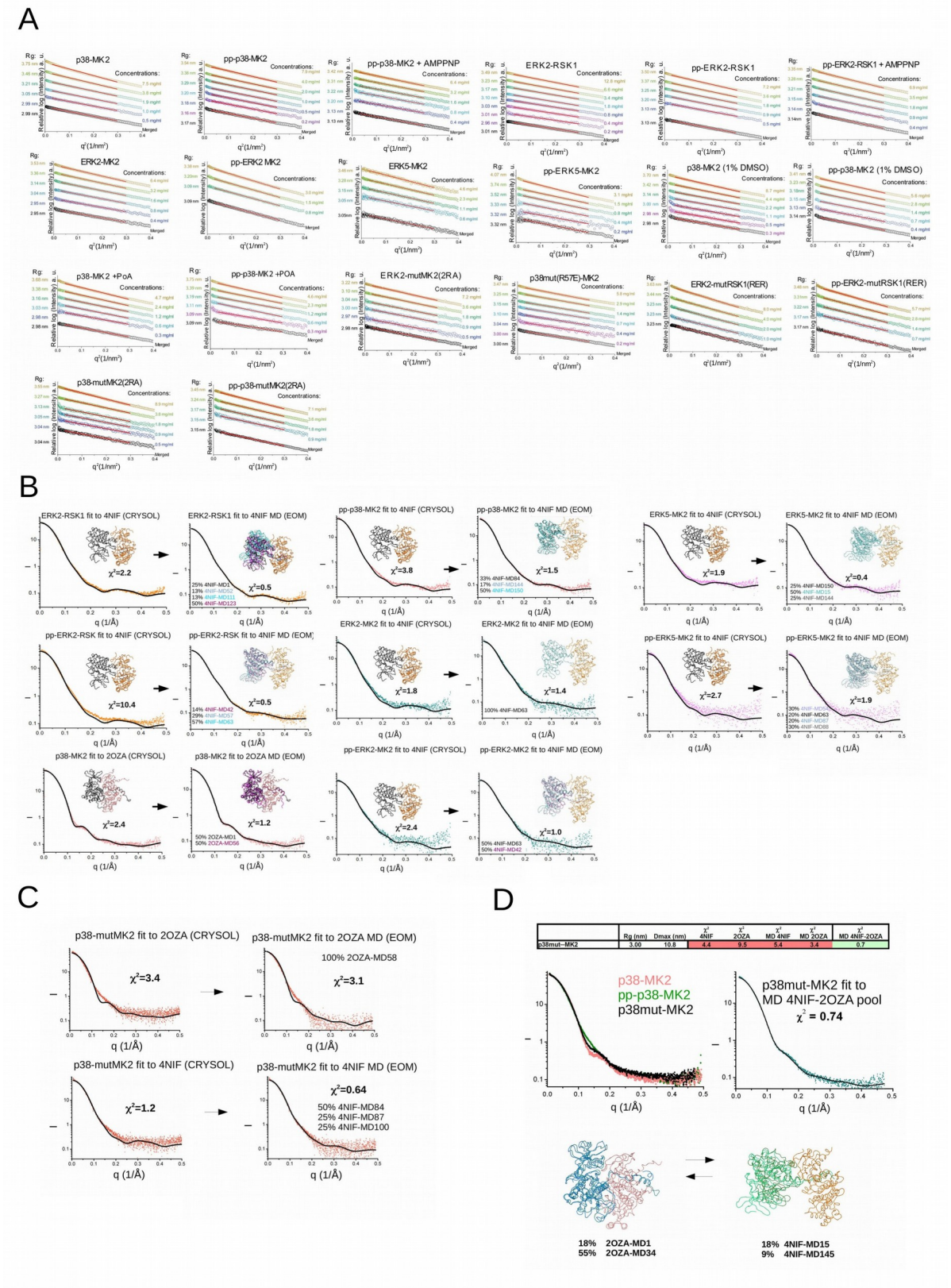

	Rg (nm)	Dmax (nm)	χ^2 4NIF	χ^2 2OZA	χ^2 MD 4NIF	χ^2 MD 2OZA	χ^2 MD 4NIF-2OZA
p38mut--MK2	3.00	10.8	4.4	9.5	5.4	3.4	0.7

Figure S4. Related to Figure 3. Detailed information on SAXS data processing and model fitting

(**A**) Guinier plot analysis of SAXS data. MAPK-MAPKAPK complexes were measured in different concentrations by diluting the stock with the equilibrated buffer obtained when the concentrated stock had been dialyzed. Scattering of each examined complex is shown in the so-called Guinier representation for the whole concentration dilution series (differently colored). The Guinier region used for calculating the radius of gyration (Rg) is highlighted with a red line. The merged curve used for the final Rg calculation is shown in black. Measured data on the whole dilution series were manually merged together. Samples showed mild concentration dependent aggregation, which fortunately was not apparent under lower concentration conditions (after several two-fold dilutions).
(**B**) Single state vs. ensemble modeling. Panels on the left show the calculated curves using the ERK2-RSK1 or the p38α-MK2 crystallographic model to experimental SAXS curves for all complexes shown in the table on Figure 2D. Panels on the right: Fits to ensembles calculated by a set of 4NIF or 2OZA MD models. Calculated curves are shown in black. For the ensemble set (shown in magenta or cyan), the abundance of individual MD models (with their MD identifier number) is shown on the panels on right. The most abundant MD model is colored in magenta, others in cyan while the MD model corresponding to the crystal structure (MD1) is colored in black. Ensemble heterodimer models were superimposed via the MAPK and this aligned ensemble is shown on the right panels.
(**C**) Fit of the p38-mutMK2 experimental SAXS curve to the crystallographic complexes (CRYSOL) or to MD ensembles (EOM). Note that the wild-type p38-MK2 complex could be best fitted to the 2OZA MD ensemble, while the mutated complex fitted best to the 4NIF MD ensemble.
(**D**) SAXS analysis on the solution structure of the p38(R57E)-MK2 complex. Scattering curves for the p38(R57E)-MK2 complex (in black) and for wild-type p38 containing complexes (p38-MK2 in salmon and pp-p38−MK2 in green) are shown below the summary table on the left. MD ensemble fit for the p38(R57E)-MK2 complex is shown on the right. The best EOM fit was obtained if models were allowed to be chosen from both the 2OZA (~70% with two models) and the 4NIF MD ensembles (~30% for two models). These models from both ensembles are shown below (using the MAPK as the reference)

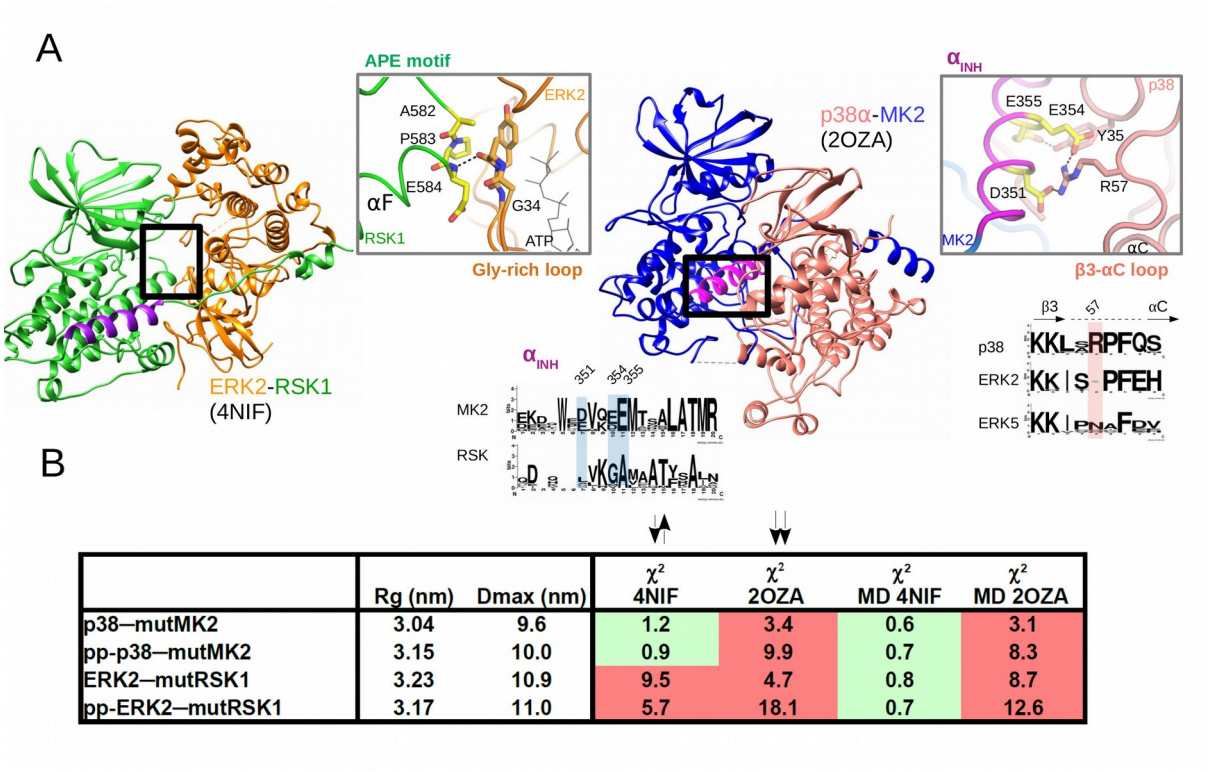

	Rg (nm)	Dmax (nm)	χ^2 4NIF	χ^2 2OZA	χ^2 MD 4NIF	χ^2 MD 2OZA
p38–mutMK2	3.04	9.6	1.2	3.4	0.6	3.1
pp-p38–mutMK2	3.15	10.0	0.9	9.9	0.7	8.3
ERK2–mutRSK1	3.23	10.9	9.5	4.7	0.8	8.7
pp-ERK2–mutRSK1	3.17	11.0	5.7	18.1	0.7	12.6

Figure S5. Related to Figure 3. SAXS analysis on p38-MK2 and ERK2-RSK1 heterodimers mutated on the parallel vs antiparalell MAPK-MAPKAPK interface
(**A)** p38α-MK2 and ERK2-RSK1 crystal structures revealed distinct heterodimeric protein-protein contacts (1,20). The C-terminal end of the αF helix from RSK1 (APE motif: Ala^{582}, Pro^{583} and Glu^{584}) contacts the Gly-rich loop of ERK2 (G34-G37) in the inactive ERK2-RSK1 complex, where a backbone mediated hydrogen bond forms between these kinase regions. The CAMK inhibitory helix is colored in magenta, hydrogen bonds are highlighted with dashed lines and ATP bound in the nucleotide binding pocket is shown in gray. In contrast to this, negatively charged residues from the inhibitory helix of MK2 (Asp^{351}, Glu^{354} and Glu^{355}) and two amino acids from p38α (Arg^{57}, Tyr^{35}) form side-chain specific intermolecular hydrogen bonds in the inactive p38α-MK2 complex. Sequence logos below show the evolutionary sequence conservation of MAPK and MAPKAPK regions engaged in the parallel p38-MK2 heterodimer. Arg^{57} of human p38α (highlighted in pink) is conserved in all orthologs. The autoinhibitory helix of MK2 contains negatively charged residues (Asp^{351}, Glu^{354}, Glu^{355}; highlighted in blue). Logos were made based on orthologs from sponge through flat worm, worm, insects to vertebrates (e.g. fish, frog, reptile, bird, human).
(**B**) SAXS data analysis on MAPK-MAPKAPK heterodimers with MK2 or RSK1 interface mutants. Note that in contrast to wild-type p38α-MK2 (parallel), the p38α-mutMK2 complex adopts an antiparallel heterodimer. However, the ERK2-mutRSK1 complex stays antiparallel but fits to different MD models compared to the wild-type heterodimer.

	Rg (nm)	Dmax (nm)	χ^2 4NIF	χ^2 2OZA	χ^2 MD 4NIF	χ^2 MD 2OZA
p38–MK2	2.99	9.4	4.6	2.4	8.9	1.2
p38–MK2 + PoA	2.98	9.6	3.6	1.6	4.5	1.1
pp-p38–MK2	3.16	10.7	3.8	23.2	1.5	26.7
pp-p38–MK2 + PoA	3.09	10.3	2.2	2.1	2.7	1.1
p38–MK2 + DMSO	2.98	9.5	5.8	3.1	9.9	0.9
pp-p38–MK2 + DMSO	3.14	10.4	37.6	77.3	1.1	18.3
pp-p38–MK2 + AMPPNP	3.13	10.4	2.4	15.3	1.2	9.9

Figure S6. Related to Figure 5. SAXS analysis on the effects of PoA binding to p38-MK2 and pp-p38-MK2 heterodimers

SAXS analysis of p38-MK2 complexes bound to the PoA inhibitor. The upper part of the table shows the summary of the SAXS analysis with PoA and the lower part with some control compounds. Note that the p38-MK2-PoA sample fit well to the inactive p38-MK2 complex (2OZA). The crystal structure of the ternary complex was also determined (PDB ID: 4TYH) and was found to be basically identical to the inactive binary complex. Unexpectedly, the pp-p38-MK2-PoA ternary complex fit neither to parallel nor to antiparallel crystallographic heterodimers, but a good fit to structures from the parallel MD 2OZA ensemble suggests that this complex adopts a parallel quaternary structure. In contrast, samples with DMSO or AMPPNP fit to antiparallel heterodimers as expected. These two latter samples were analyzed to show that PoA affects MAPK-MAPKAPK heterodimerization in a specific and unique way, and the observed changes are not due to the presence of DMSO (2%; as ternary complex samples with the PoA inhibitor contained this amount of organic solvent) or because of the nucleotide binding pocket is filled up by a small molecule (e.g. by a non-hydrolyzable ATP analogue, AMPPNP). SAXS data for the p38-MK2 and the pp-p38-MK2 binary complexes on this figure are the same as presented on Figure 3C.

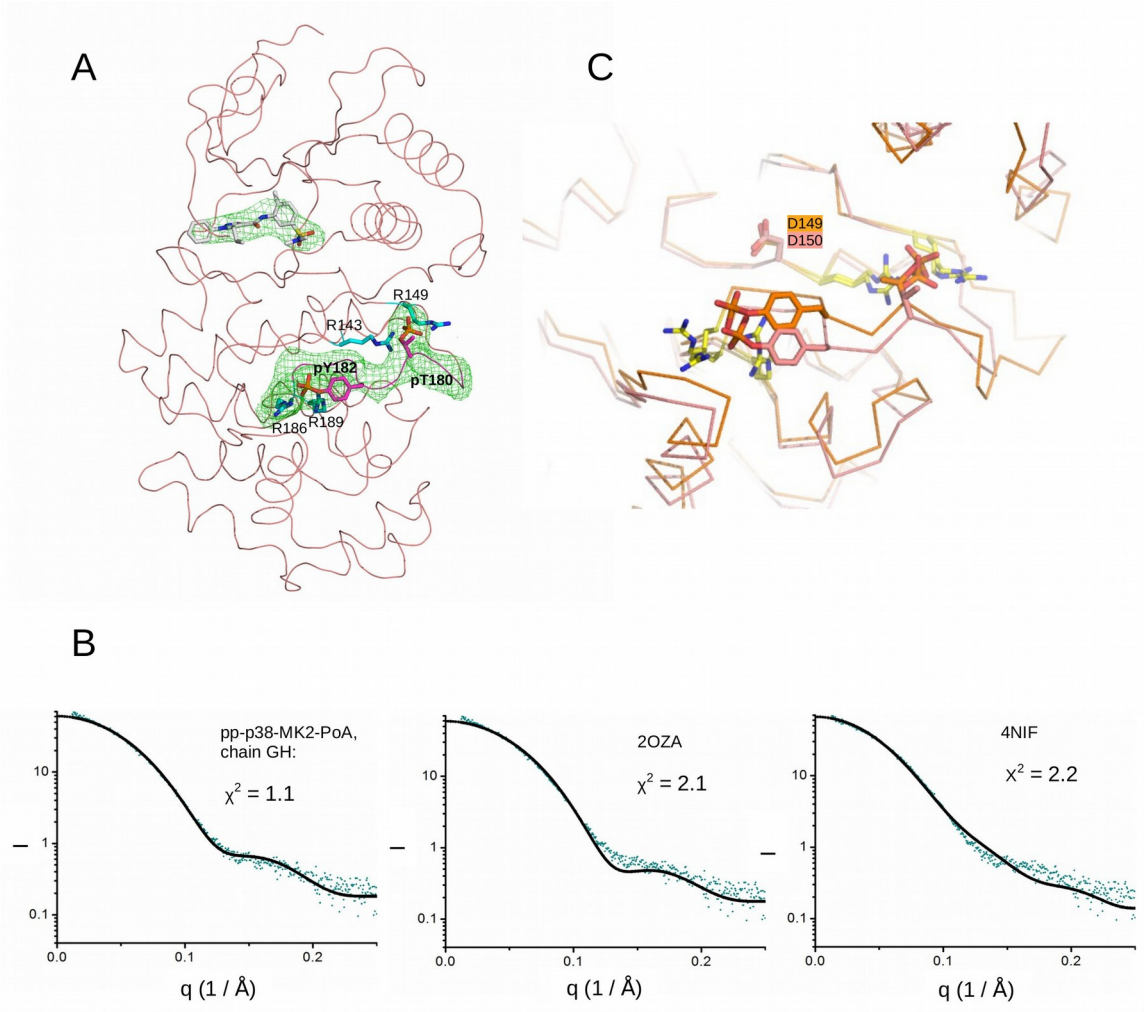

Heterodimer	χ^2
2OZA	2.1
AB	1.6
CD	1.4
EF	1.5
GH	1.1

Figure S7. Related to Figure 6. Details of the pp-p38-MK2-PoA ternary complex crystal structure

(A) SigmaA-weighted omit map contoured at 2σ for the PoA inhibitor (in gray) and sigmaA-weighted omit map contoured at 2σ for the phosphorylated p38 activation loop (177-186, in magenta). Arg^{149}, Arg^{173} and Arg^{186}, Arg^{189} coordinating phospho-Thr^{180} or phospho-Tyr^{182}, respectively, are colored in cyan. The main chain ribbon for p38 is shown in orange.

(**B**) CRYSOL fits between the SAXS data collected on the pp-p38-MK2-PoA ternary complex and different crystallographic MAPK-MAPKAPK heterodimers: chain AB, CD, EF,

GH from the new pp-p38-MK2-PoA ternary complex, 2OZA or 4NIF crystallographic models. This analysis showed that any of the four crystallographic heterodimers fit the solution structure better than the heterodimer from the inactive p38-MK2 crystallographic complex (2OZA or 4TYH). Surprisingly, the SAXS data matched best to a heterodimer that differed most from the inactive p38-MK2 crystallographic model (chains GH).
(**C**) Comparison of the pp-p38 (in salmon) and pp-ERK2 (PDB ID: 2ERK, in orange) activation loops. Phospho-amino acids are coordinated similarly by arginines (in yellow), therefore the C-terminal half of the activation loop – which blocks access to the catalytic aspartate in the inactive form - is anchored to the C-lobe and contributes to the formation of an open substrate binding pocket.

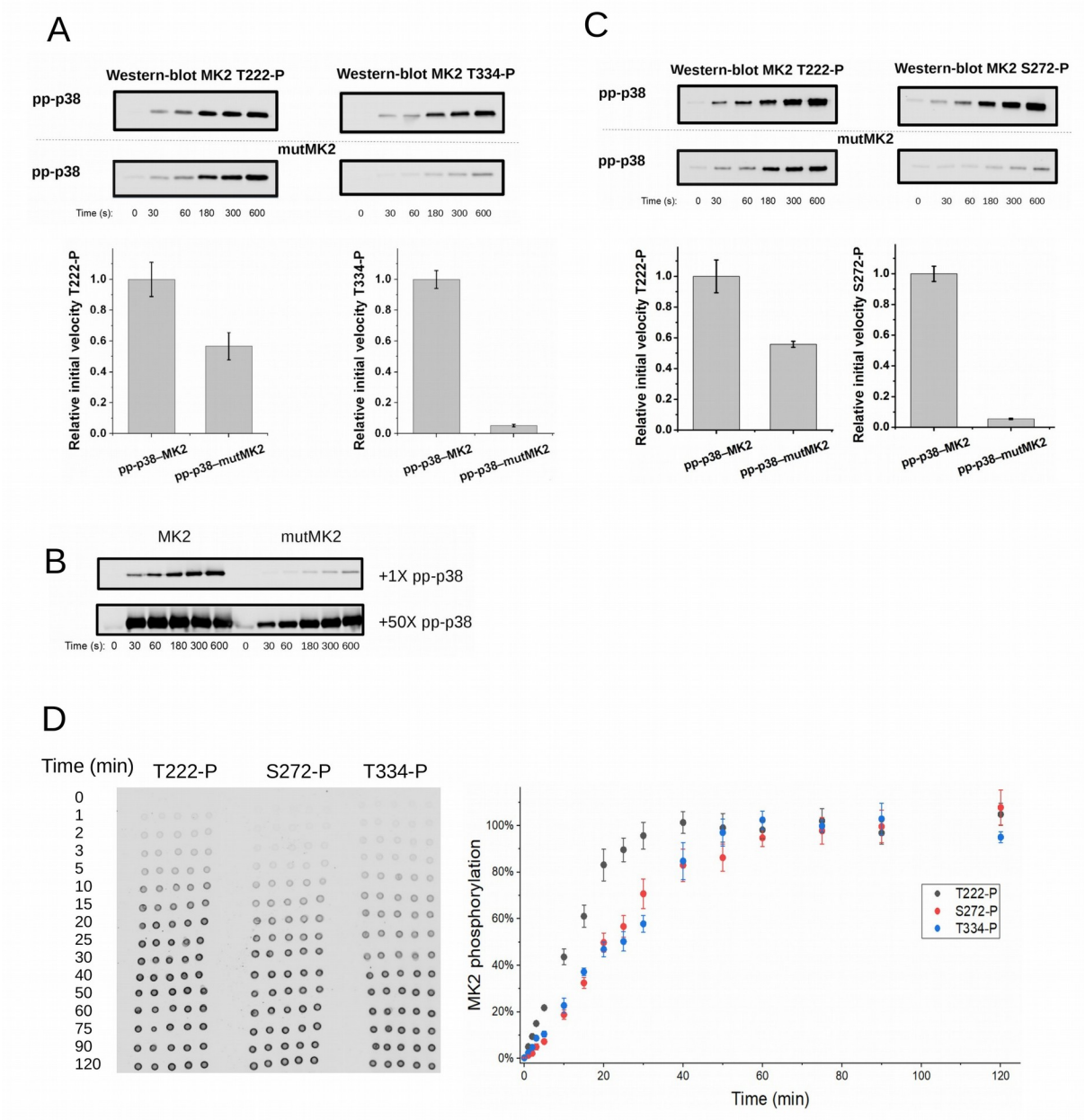

Figure S8. Related Figure 7. AL (Thr-222), Ser-272, and Thr-334 phosphorylation of MK2 by p38

(**A**) Phosphorylation of MK2 at Thr^{334} and Thr^{222} by pp-p38. Quantitative Western-blot (WB) analysis was used to monitor phosphorylation of T334 in comparison to phosphorylation at Thr^{222} (activation loop). 3 nM of pp-p38 was incubated with 2 μM MK2 (or mutMK2). The initial rate of phosphorylation at these two different MK2 sites was linearly fitted and plotted in the graph below. Error bars show SD for three independent experiments and WB panels show a representative set.

(**B**) Phosphorylation of MK2 by activated p38 on Thr^{334} – Western blot signal control. This control experiment demonstrates that amino acid replacements in mutMK2 (D351A/E354R/E355R) do not interfere with the epitope binding capacity of the phosphoMK2(T334) antibody. Note that 50-fold more activator (pp-p38) gives equally strong

WB signal with mutMK2 as with wild-type MK2. (1X: 5 nM pp-p38; MK2 concentration was 2 μM)
(**C**) Phosphorylation of MK2 at Ser^{272} and Thr^{222} by different activated MAPKs. Quantitative Western-blot (WB) analysis was used to monitor phosphorylation of S272 in comparison to phosphorylation at Thr^{222} (activation loop). The experiments were done similarly as for Panel B, but the anti-phosphoS272-MK2 antibody, in addition to phosphoT222, was used as the WB read-out.
(**D**) Kinetics of MK2 phosphorylation at T222, S272 or T334 by pp-p38.
In vitro kinase assay reactions were carried out using 2.5 mM ATP, 1 nM pp-p38 and 1 μM MK2. The reaction was stopped by adding 50 mM EDTA. Samples were collected in different time points until 2 hours. Five parallel aliquots were dotted onto the membrane for every time points and dot-blots were analyzed using phospho-T222, phospho-S272, or phospho-T334 specific MK2 antibodies. Western-blot signal was analyzed using Odyssey CLx imaging system (Li-Cor), where measured WB signal fell within the linear range of the detection, which was checked by using a calibration series of fully phosphorylated MK2. All MK2 site phosphorylation reached a plateau after 60 minutes. These maxima (100%) were used to normalize the WB signal so that they could be compared. Error bars show SD based on five technical replicates.